Response of clay soil to three-dimensional tunnelling simulation in centrifuge models

Abstract

Tunnelling-induced ground movements are complicated and investigations into them normally require some simplifications. This paper provides a brief literature review which highlights the advantages of adopting simplifications in physical modelling and addresses some of the deficiencies in assessment of soil deformations due to the simulated tunnel excavation. A set of centrifuge tests modelling a tunnel heading located at different depths in clay was carried out at 125g. The tunnel was modelled by a semi-circular cavity which partly supported by a stiff lining. The unlined tunnel heading was supported by a thin rubber bag supplied with compressed air pressure. Tunnel excavation was simulated by reducing air pressure. The induced ground movements at subsurface and surface were measured by 2D image analysis and a new, novel 3D imaging system. The results show that the experiment successfully reproduced key aspects of tunnelling-induced soil deformation in practice. In addition, a new equation to predict horizontal displacements in the longitudinal direction is suggested.

Keywords

Centrifuge modelling; Tunnels & tunnelling;

LIST OF SYMBOLS

3D	three-dimensional
3DIS	three-dimensional imaging system
a	tunnel radius
C	cover depth above tunnel
D	tunnel diameter
i_x	settlement trough length parameter
i_y^z	settlement trough width parameter at depth z
K	dimensionless parameter
g	acceleration due to gravity (9.81m/s^2)
$G()$	function of the normal probability curve
LF	Load factor
N	Tunnel stability ratio
N_{TC}	Tunnel stability at collapse
P	unlined portion of tunnel heading
PIV	Particle Image Velocity
u	horizontal displacement in X direction
v	horizontal displacement in Y direction
V_L	volume loss
V_S	volume of settlement trough
V_{ex}	volume of excavation
w	vertical displacement in Z direction
z	depth from soil surface
z_0	depth of tunnel centreline from the ground surface
γ	unit weight of soil (kN/m^3)
σ_T	tunnel support pressure
σ_{ob}	overburden stress at tunnel centreline
δ	soil displacement in spherical cavity contraction
TBM	Tunnel Boring Machine
EPBM	Earth Pressure Balance Machine

INTRODUCTION

The movement idealisation of soil displacements resulting from tunnel excavation in practice is illustrated in **Fig 1**. Observations from field measurements have demonstrated that settlement troughs in the transverse direction for single tunnel projects are nearly symmetric and that the increase in the magnitude of soil settlement after the tunnel face has passed the measurement line by a distance of a tunnel depth, z_0, is often negligible (Attewell & Woodman, 1982; Nyren, 1998). Therefore, a simple 2D plane strain model can be used to study soil deformations behind the tunnel shield. Many authors (Peck, 1969; O'Reilly and New, 1982) demonstrated that the transverse surface settlement trough caused by tunnelling can be well described by a Gaussian distribution;

$$w = w_{max} exp\left(\frac{-y^2}{2i_y^2}\right) \quad (1a)$$

$$w_{max} = V_S/\sqrt{2\pi}i_y; \quad (1b)$$

where w is surface settlement,

y is the distance from the tunnel centre line to the settlement point in the transverse direction (along the Y direction in **Fig 1**),

w_{max} is the maximum settlement (usually corresponding to $y = 0$),

i_y is the distance from the centreline to the point of inflexion in the transverse direction (along the Y direction in **Fig 1**),

V_s Volume of settlement trough.

Previous studies, using centrifuge modelling techniques with 2D models, were shown to be capable in reproducing soil responses similar to tunnelling-induced displacements, including the shape of the Gaussian settlement curve and the development of settlement with depth (Grant, 1998; Marshall, 2009; Divall, 2013). One drawback of a plane strain 2D model is that it does not take into account ground movements into the tunnel face (component 1-a in **Fig 1**), and only movements in the plane perpendicular to the tunnel centreline are simulated. To some extent, this may affect the distribution of the soil movements. More importantly, in cases where non-

57 axisymmetric characteristics of soil displacements due to tunnelling is important then a 3D
58 model is required.
59
60 In some studies, efforts were made to conduct full 3D modelling of an advancing tunnel using a
61 miniature TBM in centrifuge modelling (Hisatake & Ohno, 2008) and at 1g (Bel *et al*.,2015).
62 These studies had the intention of simulating the excavation process of a TBM hence soil
63 displacements due to tunnel advance were expected to be replicated. However, fabricating a
64 miniature TBM and incorporating this into a physical model is not a straightforward task.
65 Moreover, soil displacements data from Hisatake & Ohno (2008) and Bel *et al*., (2015) were
66 limited to settlement at the surface only and no subsurface soil deformations were reported.
67 These might have been attributed to the complexity of having the miniature TBM which
68 obstructed sophisticated measurement systems that might have been used to obtain subsurface
69 deformations and horizontal displacements at the surface.
70
71 Those difficulties in conducting full 3D models required simplifications to be adopted in
72 simulating the tunnel excavation process in physical models while allowing the full distribution of
73 the induced soil deformations to be observed. The use of centrifuge modelling to investigate the
74 effects of non-axisymmetric characteristics of tunnelling-induced soil displacements or soil
75 reinforcement measures (spiles or forepoles systems) were reported by Mair (1979), Calvello &
76 Taylor (1999), Date *et al*., (2008), Yeo (2011), Boonyarak & Ng (2014), and Le & Taylor (2016).
77 However, little information on the similarities between the observed soil displacements in the
78 experiments with those in tunnelling practice were provided which is deemed necessary to
79 support the findings obtained from the test results.
80
81 This paper presents the results from a set of centrifuge tests featuring a 3D tunnel heading
82 located at different depths along with empirical predictions and sophisticated field measurement
83 data from previous publications.
84

CENTRIFUGE TEST

Test series

Two centrifuge tests simulating a 3D tunnel heading at two different depths $C/D = 1$ and $C/D = 3$ in clay were conducted. The test details are presented in **Table 1**. A schematic of a typical centrifuge test is illustrated in **Fig 2**.

Model tunnel

The tunnel was simulated by a 190mm long, 50mm diameter semi-circular cavity cut in the front face of the model clay which formed a plane of symmetry of the tunnel heading. That allowed subsurface soil deformations in this plane, which were expected to be the largest, to be measured. The model was partly supported by a 165mm long stainless steel lining which left the unlined heading $P = 25$mm to be supported by a thin rubber bag supplied with compressed air pressure. The ratio $P/D = 25/50 = 0.5$ was chosen because it is within the range of $P/D = 0.1 - 1$ which was reported in many case studies (Macklin, 1999; Dimmock, 2003). All the tests were conducted at *n*=125g. At this acceleration, the corresponding prototype scale tunnel geometries are as presented in **Table 1**.

Model container and potential boundary effects

The internal dimensions, 550mm (L) x 200mm (W) x 375mm (H), of the model container allow centrifuge tests with normalised tunnel depth up to C/D=3 which is considered adequate to cover different soil deformation mechanisms (Davis et al., 1980).

Regarding boundary effects, the distance, in transverse direction, from the centreline of the model tunnel to the side of the container in this study is 200mm/50mm=4D which is larger than the minimum distance of 3D suggested by Kimura & Mair (1981). The depth of the model clay beneath the invert of the model tunnel was more than 1D, the minimum value suggested by Taylor (1995). The distance from the tunnel face to the side wall of the container, in longitudinal direction, was 165mm which was larger than 3*D*. Therefore, minor effects of the boundary to soil displacements in the centrifuge model can be expected.

Clay model

Speswhite kaolin power was mixed with distilled water, in a ribbon mixer, to produce a uniform mixed slurry of moisture content at approximately 120%. At this moisture content, the clay particles are free to develop their own structure under applied stress (Mair, 1979). Properties of Speswhite kaolin are presented in **Table 2**. Prior to pouring the slurry into the model container, grease was applied to the container's side walls to reduce friction. Two sets of 3mm porous plastic sheet and a filter paper were placed at the bottom and the top of the sample to enable dual drainage paths to shorten the required time for consolidation. The model container was then placed under a hydraulic press to one dimensionally consolidate the sample to a maximum vertical effective stress σ'_{v0}=175kPa.

The consolidation pressure σ'_{v0}=175kPa was chosen as it provided soft clay model in which the soil deformations, induced by the simulated tunnel excavation, would be large and can be observed clearly (Le, 2017). In addition, with a preconsolidation pressure σ'_{v0}=175kPa, the clay above the tunnel axis level in the centrifuge test is overconsolidated (Le, 2017) which is similar to most of soil clays in practice (Parry, 1969). It is worth noting that the OCR of soils around the tunnel in test CD1 and CD3 were different due to the different overburden depth. However, the difference in OCR did not cause any noticeable effects to the shape of soil displacement profile as shown in the test results section.

Instrumentation

For test CD1, a row of displacement transducers was used to measure surface settlements and the image analysis program Visimet (Grant, 1998) was used to measure subsurface soil movements. For test CD3 which was conducted later, a new 3D imaging system (Le et al., 2016) was developed and used to measure 3D soil displacements at the model surface while GeoPIV_RG (Stanier *et al*., 2015) was used to measure subsurface soil deformations. The changes in pore pressure were measured by Pore Pressure Transducers (PPTs), model PDCR81 supplied by Druck Limited Leicester, which were installed within the soil model. The air support pressure in the tunnel bag was measured by a model PX600-200GV series pressure transducer, supplied by Omega Engineering Ltd.

Test procedure

On the test day, the clay sample was removed from the hydraulic press and trimmed to the correct height. The top surface and the front face of the clay were coated respectively by Plasti Dip and silicone fluid to prevent moisture loss. For test CD3, Leighton Buzzard Sand faction E was used to create texture to aid the 3DIS analysis (Le *et al*., 2016). The tunnel cavity was cut which then allowed the model lining and rubber bag to be put into place. Targets or texture material (glass ballotini) were embedded into the front face of the model for later image analysis to determine subsurface displacements using Visimet (Grant, 1998) or GeoPIV_RG (Stanier *et al*., 2015). The front perspex window was coated by high viscosity silicone fluid to minimise friction with the clay sample before being firmly bolted into the model container.

The models were accelerated to 125g while the tunnel air pressure, σ_T was simultaneously increased to support the overburden stress at the equivalent centrifugal gravity, *n*.

$$\sigma_{ob}=\gamma z n \tag{2}$$

where

σ_{ob}: overburden stress at depth z,

γ is the unit weight of soil.

It is worth noting that the tunnel air support pressure within the tunnel heading was equal in all directions whereas soil pressure increases with depth. If σ_T was chosen to balance σ_{ob} at the tunnel axis level $z = C + D/2$ then the upper part of the tunnel would be over pressurised. Therefore, it was decided to choose σ_T to balance σ_{ob} near the tunnel crown at depth $z = C + D/4$ which was shown to be adequate to keep the tunnel heading stable, without significantly over pressurising the upper part of the tunnel. For CD1 and CD3 tests, the initial tunnel support pressure at 125g were σ_{T0}= 129kPa and σ_{T0}= 335kPa respectively.

It is worth to note that the effects of the difference in soil stress and the initial air support pressure in the tunnel heading was negligible. Good agreement between field measurement

and centrifuge test results on the pattern of soil displacements are presented later in this paper, in addition to observation made by previous research (Mair, 1979; Grant, 1998; Divall, 2013).

The air support pressure was controlled using a valve in the centrifuge control room and full details, including drawings and diagrams, can be found in Le (2017). After the excess pore pressure dissipated and the clay consolidated, the tests were started by gradually reducing the air support pressure from σ_{T0}, at a rate of approximately 2kPa/s, to zero to simulate the tunnel excavation process. Data from the LVDTs, and pressure transducer, and digital images were recorded at 1 second intervals for later analysis.

TEST RESULTS

An example of surface (from 3DIS) and subsurface (from GeoPIV_RG) displacement data for test CD3 is illustrated in **Fig 3**. The definition of the coordinate system and displacement convention is also presented.

Settlement trough in the transverse direction

A typical settlement trough at the model surface is illustrated in **Fig 4** together with a corresponding Gaussian curve (**Equation 1a**). The best fit method proposed by Jones & Clayton, (2013) was used to estimate the settlement trough width for different stages of the test which gave $i_y \approx 85$mm. The corresponding dimensionless parameter $K = i_y/z = 85/175 = 0.49$. This K value falls within the common range of typical $K = 0.4 \div 0.7$ for many case histories of tunnelling in clay (O'Reilly & New, 1982). Good agreement between the experimental and the empirical Gaussian curves can be seen in **Fig 4**.

Horizontal displacement in transverse direction

In practice, horizontal movements are difficult to measure and relatively few data from case histories have been published. **Fig 5** compares the trend of horizontal soil displacement in test CD3 with field measurements from Hong & Bae (1995) and Nyren (1998) and the empirical profile proposed by O'Reilly & New (1982);

$$v_y = \frac{y w_y}{z_0} \quad (3)$$

where v_y is the horizontal displacement in the transverse direction at a distance y from the tunnel centreline,

w_y is the soil settlement at a distance y from the tunnel centreline, calculated from **Equation 1a**.

The offset from the tunnel centreline y is normalised against i_y and the horizontal displacement v is normalised against the maximum value v_{max}. It is evident that the maximum value v_{max} occurs at an offset of approximately $y = i_y$ from the tunnel centreline. It can be seen that the experimental data are consistent with previously published field data and both are well presented by **Equation 3**. This consistency also implies that the boundary effect was negligible which further corroborates the suggested minimum distance to the boundary from tunnel centreline of 3D (Kimura & Mair, 1981).

Longitudinal soil surface settlement above the tunnel centreline

Previous authors (Attewell & Woodman, 1982; Nyren, 1998; Dimmock, 2003) demonstrated that, regardless of the tunnel construction technique and tunnel depth, the measured longitudinal surface soil settlement in front of an advancing tunnel was well represented by the cumulative probability function (**Equation 4**) proposed by Attewell & Woodman (1982);

$$w_x = w_{final} \left\{ G\left(\frac{x - x_i}{i_x}\right) - G\left(\frac{x - x_f}{i_x}\right) \right\} \quad (4)$$

where w_{final} is the final surface settlement above the tunnel centreline;

i_x is the settlement trough length parameter;

x_i is the initial or tunnel start point (y = 0);

x_f is the tunnel face position (y = 0);

$G()$ is the function of the normal probability curve;

For the model tunnel heading in the centrifuge tests, it is reasonable to consider that the start point x_i and tunnel face position x_f respectively coincide with the edge of the tunnel lining and the end of the unlined heading as depicted in **Fig 6-a**. The required variables to define the longitudinal surface settlement profile above the tunnel centreline are the final surface settlement w_{final} and settlement trough length parameter i_x.

It is reasonable to consider the final surface settlement w_{final} as a constant and the normal assumption is that the settlement directly above the tunnel face, w_{face} is $0.5w_{final}$. Therefore, the dimensionless profile of the longitudinal surface settlement above a tunnel centreline can be obtained by normalising w_x against w_{face} (**depicted in Fig 6-a**). The best-fit method (Jones & Clayton, 2013) was used to estimate the value of settlement trough length as $i_x/\mathrm{z}_0 = 0.46$ for both C/D=1 and C/D=3 tests. **Fig 6-b** shows a good fit between the empirical and the measured longitudinal settlement profiles in the centrifuge tests for both depths $C/D = 1$ and $C/D = 3$. This suggests that the ratio i_x/z_0 was the same for same soil, in this study Speswhite kaolin, and the tunnel depth z_0 has almost no influence. It is also evident that the surface settlement is very small at a longitudinal distance corresponding to z_0 from the tunnel face.

Settlement with depth

Fig 7-a illustrates settlement with depth obtained from extensometers, located in the vertical plane of symmetry of the tunnel centreline, with respect to the advance of the west bound tunnel at St James's Park site for the Jubilee line extension project (Nyren, 1998). The tunnel, situated in London Clay, was bored by open-face shield and mechanical backhoe. It can be seen that settlement with depth in front of the tunnel face appears to be small and the difference in magnitude of settlements at various depths were negligible. However, for settlements behind the tunnel face, the magnitude of soil settlement w_z increased with depth z. A similar trend was also observed for EPBM tunnelling in London Clay (Wan et al., 2017). Soil displacements due to the simulated tunnel excavation in the centrifuge test are presented in **Fig 7-b**. It is evident that the trend of settlement with depth in front of and behind the tunnel face in the centrifuge test and this case history are similar.

Previous authors (Mair *et al*., 1993; Nyren, 1998; Dimmock 2003; Wan et al., 2017), with extensive data from centrifuge modelling and field measurements in tunnels constructed by open-face tunnelling or TBM, showed that the profile of settlement with depth behind the tunnel face was well predicted by Mair *et al*., (1993);

$$\frac{i_y^z}{z_0} = 0.175 + 0.325\left(1 - \frac{z}{z_0}\right) \quad (5)$$

The settlement trough width at the surface i_y^0=87.5mm (determined using **Equation 5** with *z*=0) is consistent with the estimated $i = 85mm$ based on the experimental transverse settlement trough. Combining **Equations 1a, 1b** and **5** give soil settlements with depth in the vertical plane of symmetry of the tunnel centreline ($y = 0$) as;

$$w_z = V_S/\sqrt{2\pi}i_y^z \quad (6)$$

where i_y^z is the settlement trough width parameter at depth z.

Fig 8 compares the profiles of the empirical and the measured settlement with depth for the tests CD1, CD3 and field measurement from Nyren (1998). The fit between the measured and the empirical profiles is very good except for the settlement near the depth $z/z_0 = 0.8$. Mair *et al.,* (1993) also suggested that their equation was established based on many field measurements but only a few data points were available in the area near the tunnel centreline (i.e. when $z/z_0 \geq 0.8$) and caution should be exercised with the prediction at this depth.

Longitudinal horizontal soil displacement

Fig 9 compares profiles of horizontal displacement with depth at different distances in front of tunnel face in the centrifuge tests with field measurements from a tunnel constructed using the NATM method (Clayton *et al*., 2000). In **Fig 9**, the depth of the measured point, z, is normalised by the tunnel depth z_0 and horizontal displacement, u, is normalised by the maximum horizontal displacement in the profile, u_{max}. Interestingly, despite the difference in the normalised tunnel depth C/D, the tunnel diameter and soil strength, most of the data points in the horizontal

displacements with depth profile in the centrifuge tests and field measurements, when plotted in the manner as in **Fig. 9**, shows good agreement. A Gaussian distribution curve expressed by **Equation 7** is also superimposed in **Fig 9**;

$$\frac{u}{u_{max}} = \exp\left\{-16\left(\frac{z}{z_0} - 1\right)^2\right\} \quad (7)$$

It can be seen that the Gaussian curve (Equation 7) fits well with the data especially with the field measurements. This suggests that if the horizontal displacement at the tunnel axis level is known, then the profile of longitudinal displacement at any depth can be estimated using **Equation 7**.

Mair & Taylor (1993) and Mair (2008) demonstrated that a simple linear elastic perfectly plastic model (Mair & Taylor, 1993) provided reasonable predictions of longitudinal horizontal displacement at tunnel axis level in front of a tunnel face. In their model, soil deformations in front of an advancing tunnel heading can be idealised as being consistent with the contraction of a spherical cavity in which displacement is given as;

$$\frac{\delta}{a} = \frac{S_u}{3G}\left(\frac{a}{r}\right)^2 \exp(0.75N - 1) \quad (8)$$

$$N = \frac{\sigma_{ob} - \sigma_T}{S_u} \quad (9)$$

where δ is the soil displacement at radius r; in this paper $\delta = u$

a is the inner radius of the cavity (tunnel) i.e. $0.5D$,

G is the elastic shear modulus (for isotropic conditions, the undrained Young's modulus $E_u = 3G$),

N is the stability ratio (Broms & Bennermark, 1967),

S_u is the undrained shear strength of clay,

σ_{ob} is the overburden stress at tunnel axis level,

σ_T tunnel support pressure.

The required parameters to calculate u/a at a distance of a/r in front of the tunnel face are the tunnel stability N which can be calculated using **Equation 9** and the ratio $S_u/3G$. While S_u can be measured by hand shear vane on the soil model post-test, obtaining an accurate and reliable soil stiffness, G, in a centrifuge model is not a straight-forward task hence no further analysis was carried out. Nevertheless, from **Fig 10** it is evident that u/a is linear with a/r as observed in a field measurements reported by Mair & Taylor (1993) and Mair (2008).

3D Volume loss

In the conventional tunnelling framework, volume loss V_L is referred to as the two dimensional cross-sectional area of the settlement trough when the tunnel excavation has been completed and is often expressed as a percentage of the tunnel area excavated. This volume loss can be predicted using the Load Factor method given by **Equation 10** which was proposed by Macklin (1999);

$$V_L = 0.23e^{4.4(LF)}; \text{ for } LF \geq 0.2 \quad (10)$$

$$LF = N/N_{TC} \quad (11)$$

$$N_{TC} = \frac{\sigma_{ob} - \sigma_{TC}}{S_u} \quad (12)$$

where LF is load factor,

N is tunnel stability ratio (Broms & Bennemark, 1967) (**Equation 9**),

N_{TC} is the stability ratio at collapse (**Equation 12**).

σ_{TC} is the tunnel support pressure at collapse.

By means of 3DIS, the volume of the settlement trough in 3D induced by the reduction of tunnel support pressure in the centrifuge test was measured which enables the developing 3D volume loss to be calculated by **Equation 13**;

$$V_L = \frac{V_S}{V_{ex}} \ (\%) \quad (13)$$

$$V_{ex} = \left(\frac{\pi D^2}{2 \times 4}\right) P \ (mm^3) \quad (14)$$

(Note – only a half section of tunnel is modelled in these tests)

where V_S: volume of the settlement trough in 3D measured by 3DIS (mm^3),

V_{ex}: volume of the excavation in 3D (mm^3) corresponding to the unlined heading *P*.

This approach to 3D volume loss gives an opportunity to assess if the Macklin (1999) method is applicable in a 3D scenario. The tunnel support pressure at collapse σ_{TC} in test CD3 was determined as 108kPa (Le, 2017). The undrained shear strength of the clay model was estimated as S_u=31.5kPa (Le, 2017). Using $\sigma_{TC} = 108kPa$ and S_u=31.5kPa in **Equation 12** gives the stability ratio at collapse for test CD3 N_{TC}=8. This is in line with the value suggested by Kimura & Mair (1981) for a tunnel with $P/D = 0.5$ at depth of $C/D = 3$.

The relationship of the calculated LF (**Equation 11**) and the measured volume loss V_L is compared with the empirical relationship (**Equation 10**) in **Fig 11**. It is evident that most of the data points fit closely with the empirical line (solid line) and fall within the bounds proposed by Macklin (1999) (dashed lines). The results from **Fig 11** suggests that the Load Factor approach is applicable to the developing total 3D volume loss.

SUMMARY AND CONCLUSION

A relatively straight-forward centrifuge testing apparatus was used to simulate the excavation of a 3D tunnel heading in clay at two normalised tunnel depths $C/D = 1$ and $C/D = 3$. The obtained data covered soil displacements at the surface and subsurface in three-dimensions which would have not been possible in a 2D model test. High precision measurement techniques, including the novel 3D imaging system, allowed rigorous analysis and assessment of soil deformations in the centrifuge tests.

The soil movements, in horizontal and vertical directions at surface and subsurface, were found to be very consistent with those obtained from field measurements and a simplified analysis for tunnel in clay. In addition, from the test results, a new equation was proposed to predict

horizontal soil displacement in the longitudinal direction which showed reasonable agreement with field and experimental data. However, more field data are needed to confirm this finding.

The experimental evidence presented further corroborate appropriate simplifications in centrifuge modelling. That allows the complicated tunnel excavation process to be studied while ensuring the key aspects of soil displacement will be reproduced. This gives confidence that a more sophisticated experimental study, for example the effect of soil reinforcement measures or the interaction with piles and other foundations, will reveal realistic insights into tunnelling-induced soil deformations.

ACKNOWLEDGEMENTS

The first author acknowledges the Vietnam government for funding his doctoral scholarship. The authors are grateful to colleagues in the Research Centre for Multi-scale Geotechnical Engineering at City, University of London for their support.

REFERENCES

Attewell, P.B. and Woodman, J.P. (1982). Predicting the dynamics of ground settlement and its derivatives caused by tunnelling in soil. *Ground Engineering, Vol.15. No.8*, 13-22 and 36.

Bel, J., Branque, D., Wong, H., Viggiani, G. and Losacco, N., 2015. Experimental study on a 1g reduced scale model of TBM: impact of tunnelling on piled structures. Proceedings of the XVI ECSMGE Geotechnical Engineering for Infrastructure and Development.

Boonyarak, T. and Ng, C.W., 2014. Effects of construction sequence and cover depth on crossing-tunnel interaction. *Canadian Geotechnical Journal*, *52*(7), pp.851-867.

Broms,B.B. & Bennermark, H. (1967). Stability of clay in vertical openings. *J. Soil Mechanics and Foundation Division*. American Society of Civil Engineers, SM1, 71-94.

Calvello, M. & Taylor, R.N. (1999). Centrifuge modelling of a spile-reinforced tunnel heading. Proc. 2nd Int. Symp. *Geotechnical Aspects of Underground Construction in Soft Ground*. Tokyo.

387 Clayton, C.R.I., Hope, V.S., Heymann, G., Van der Berg, J.P. and Bica, A.V.D., 2000.
388 Instrumentation for monitoring sprayed concrete lined soft ground tunnels. *Proceedings of*
389 *the Institution of Civil Engineers-Geotechnical Engineering*, *143*(3), pp.119-130.
390 Date, K., Mair, R.J. & Soga, K. (2008). Reinforcing effects of forepoling and facebolts
391 in tunnelling. *Geotechnical Aspects of Underground Construction in Soft Ground –*
392 Ng, Huang & Liu (eds). Taylor & Francis Group, London
393 Dimmock, P.S. 2003. Tunnelling-induced ground and building movement on the Jubilee Line
394 Extension. PhD thesis, University of Cambridge.
395 Divall, S., 2013. *Ground movements associated with twin-tunnel construction in clay.* PhD
396 thesis, City University London.
397 Jones, B. and Clayton, C., 2013. Guidelines for Gaussian curve-fitting to settlement data. In
398 *Underground-The Way to the Future: Proceedings of the World Tunnel Congress, WTC*
399 2013 (pp. 645-652). CRC Press.
400 Grant, R.J. (1998). *Movements around tunnel in two-layer ground.* PhD thesis, City University
401 London.
402 Hisatake, M. and Ohno, S., 2008. Effects of pipe roof supports and the excavation method on
403 the displacements above a tunnel face. *Tunnelling and Underground Space Technology*,
404 *23*(2), pp.120-127.
405 Hong, S.W. and Bae, G.J., 1995. Ground movements associated with subway tunnelling in
406 Korea. *Proceedings of Underground Construction in Soft Ground. Rotterdam: AA Balkema*,
407 pp.229-232.
408 Kimura, T. and Mair, R.J., 1981, June. Centrifugal testing of model tunnels in soft clay.
409 In *Proceedings of the 10th international conference on soil mechanics and foundation*
410 *engineering* (pp. 319-322). ISSMFE: International Society for Soil Mechanics and Foundation
411 Engineering.
412 Le, B.T (2017). *The effect of forepole reinforcement on tunnelling-induced movements in clay*.
413 PhD thesis, City, University of London.
414 Le, B.T., Nadimi, S., Goodey, R.J. and Taylor, R.N. 2016. System to measure three-dimensional
415 movements in physical models. *Géotechnique Letters*, 6(4), pp.1-7.

Le, B.T. & Taylor, R. N. (2016). A study on the reinforcing capabilities of Forepoling Umbrella System in urban tunnelling. Proceeding of the 3rd European conference on physical modelling in geotechnics, Eurofuge2016, Nantes, France, pp. 325–330. Nantes, France: Ifsttar.

Macklin, S.R., 1999. The prediction of volume loss due to tunnelling in overconsolidated clay based on heading geometry and stability number. *Ground engineering*, *32*(4), pp.30-33.

Mair, R.J. (1979). *Centrifugal modelling of tunnelling construction in soft clay*. PhD Thesis, University of Cambridge.

Mair, R. J., Taylor, R. N. & Bracegirdle, A. (1993). Subsurface settlement profiles above tunnels in clays. *Geotechnique* 43, No. 2, 315-320

Mair, R.J. 2008. Tunnelling and geotechnics: new horizons. *Géotechnique*, *58*(9), pp.695-736.

Mair, R.J. & Taylor, R.N. 1993. Prediction of clay behaviour around tunnels using plasticity solutions. In *Predictive Soil Mechanics: Proceedings of the Wroth Memorial Symposium Held at St. Catherine's College, Oxford, 27–29 July 1992* (p. 449). Thomas Telford.

Marshall, A.M., *Tunnelling in sand and its effect on pipelines and piles*. PhD thesis. University of Cambridge.

Nyren, R. (1998). *Field measurements above twin tunnels in London Clay*. Ph.D. Thesis, Imperial College.

O'Reilly, M.P. & New, B.M. (1982). Settlements above tunnels in the United Kingdom -their magnitude and prediction. *Proc. Tunnelling '82 Symp., Institution of Mining and Metallurgy*, London (ed. MJ. Jones), 173-181.

Peck, R.B. (1969). Deep excavations and tunnelling in soft ground. *Proc. 7th Int. Conf. Soil Mechanics and Foundation Engineering*, Mexico, State of the Art Volume, 225-290.

Schmidt, B. (1969). *Settlements and ground movements associated with tunnelling in soil*. Ph.D. thesis, University of Illinois.

Stanier, S.A. Blaber, J., Take, W.A. & White, D.J. 2015. Improved image based deformation measurement for geotechnical applications. *Canadian Geotechnical Journal*.

444 Wan, M.S.P., Standing, J.R., Potts, D.M. and Burland, J.B., 2017. Measured short-term
445 subsurface ground displacements from EPBM tunnelling in London Clay. *Géotechnique*,
446 pp.1-32.
447 Yeo, C.H. (2011). *Stability and collapse mechanisms of unreinforced and forepole reinforced*
448 *tunnel headings*. PhD Thesis, National University of Singapore.

449 FIGURE CAPTION

450 Fig. 1: Idealisation of tunnelling induced soil displacements.

451 Fig. 2: Schematic of the centrifuge model.

452 Fig. 3: Typical soil displacements from the centrifuge test CD3.

453 Fig. 4: Typical transverse settlement trough in test CD3.

454 Fig. 5: Transverse surface horizontal soil displacement in test CD3.

455 Fig. 6: Longitudinal surface settlement above tunnel centreline.

456 Fig. 7: Settlement with depth at different locations to tunnel face.

457 Fig. 8: Settlements with depth behind tunnel face.

458 Fig. 9: Horizontal displacement in longitudinal direction.

459 Fig. 10: Horizontal displacement in longitudinal direction at tunnel axis level.

460 Fig. 11: Relationship of Load Factor, LF and volume loss VL.

Parameter	Model (mm)	Prototype (m)
Tunnel Diameter, D	50	6.25
Unlined portion, P	25	3.125
Cover depth C (C/D=1)	50	6.25
Depth at tunnel CL, z_0 (C/D=1)	75	9.375
Cover depth C (C/D=3)	150	18.75
Depth at tunnel CL, z_0 (C/D=3)	175	21.875

Table 1: Details of centrifuge test and their corresponding prototype scale tunnels.

Symbol	Parameter	Value
κ	average gradient of swelling line in v: $\ln p'$ space	0.05
λ	gradient of compression line in v: $\ln p'$ space	0.19
M	stress ratio at critical state (q': p')	0.89
Γ	specific volume at critical state when p'=1kPa	3.23
N	specific volume on INCL when p'=1kPa	3.29
φ_c'	critical state angle of shearing resistance	23°
γ	unit weight of soil (saturated for clay)	16.5 (kN/m^3)
γ_w	unit weight of water	9.81 (kN/m^3)

Table 2: Speswhite kaolin clay properties (Grant, 1998).

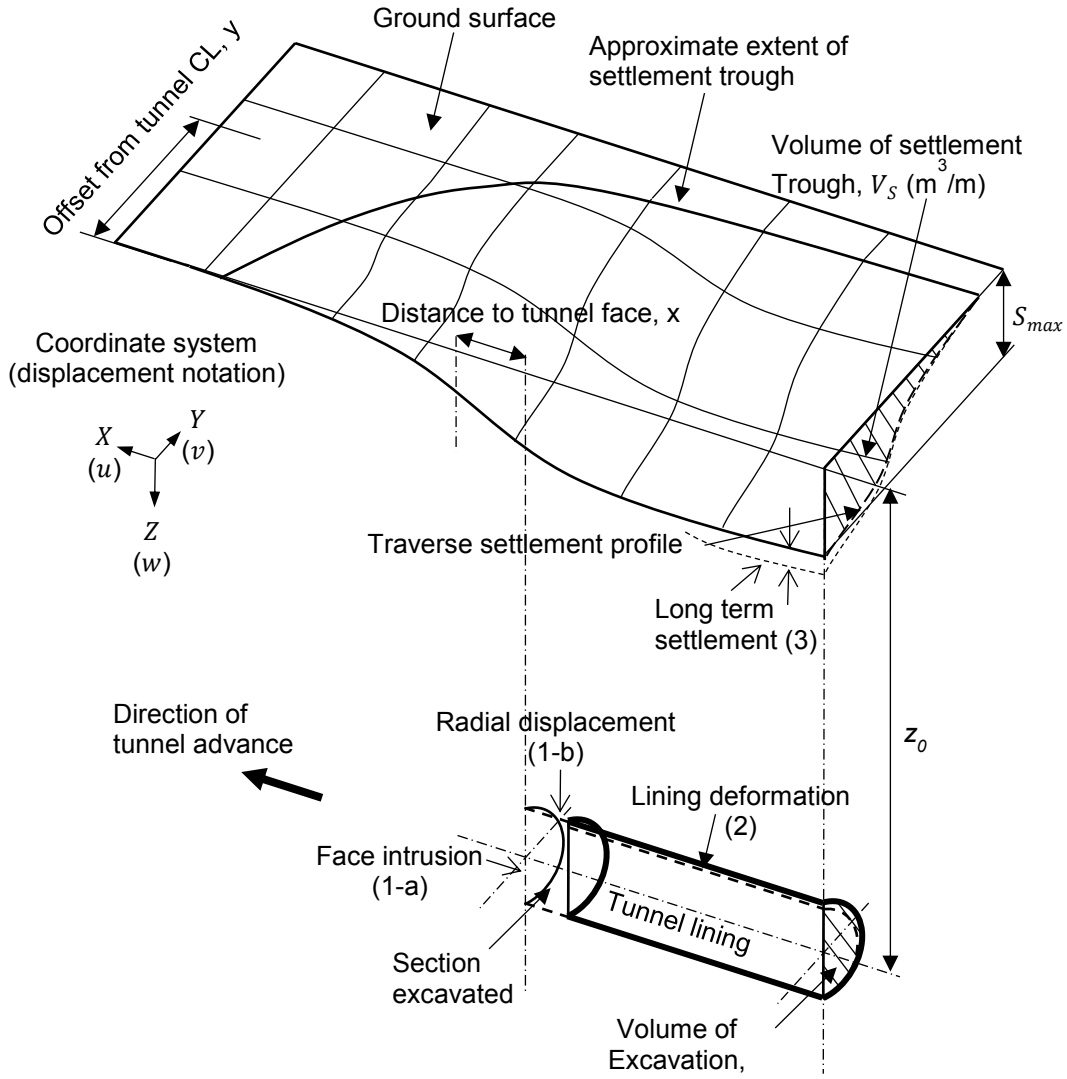

Fig. 1: Idealisation of tunnelling induced soil displacements.

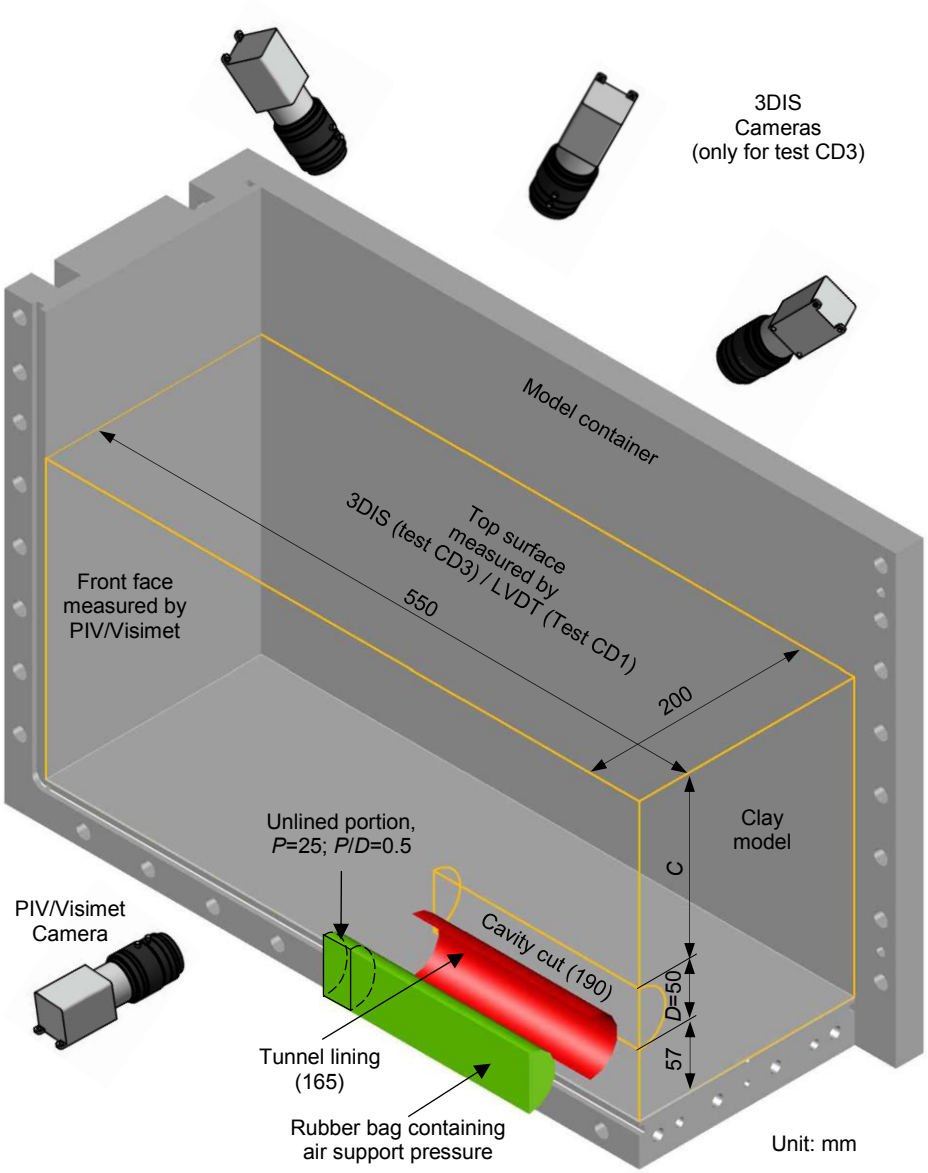

Fig. 2 : Schematic of the centrifuge model.

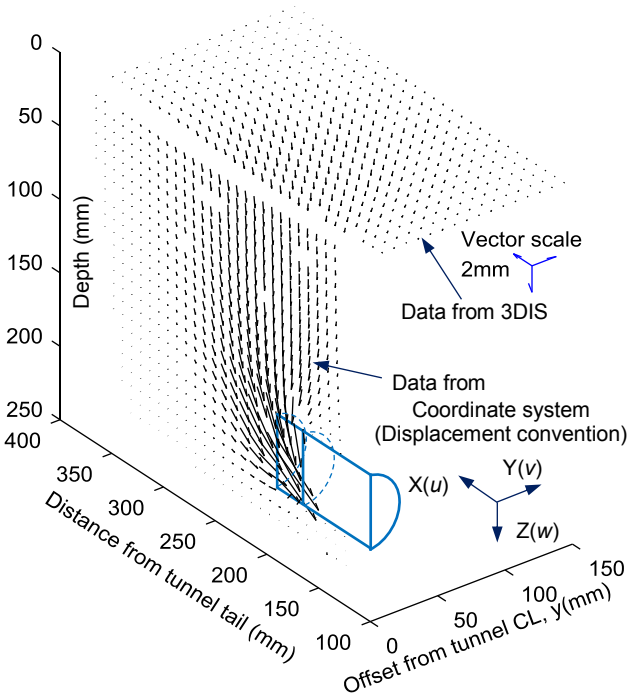

a) Soil displacements on the front face and the top surface of the model.

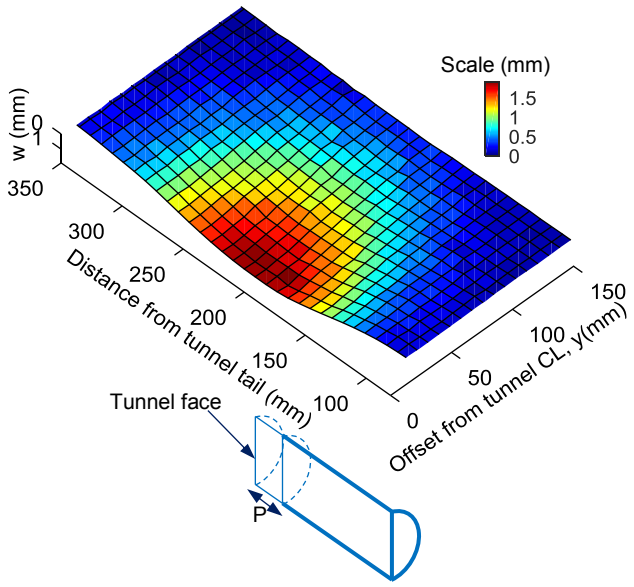

b) Typical surface settlement trough.

Fig. 3: Typical soil displacements from the centrifuge test CD3.

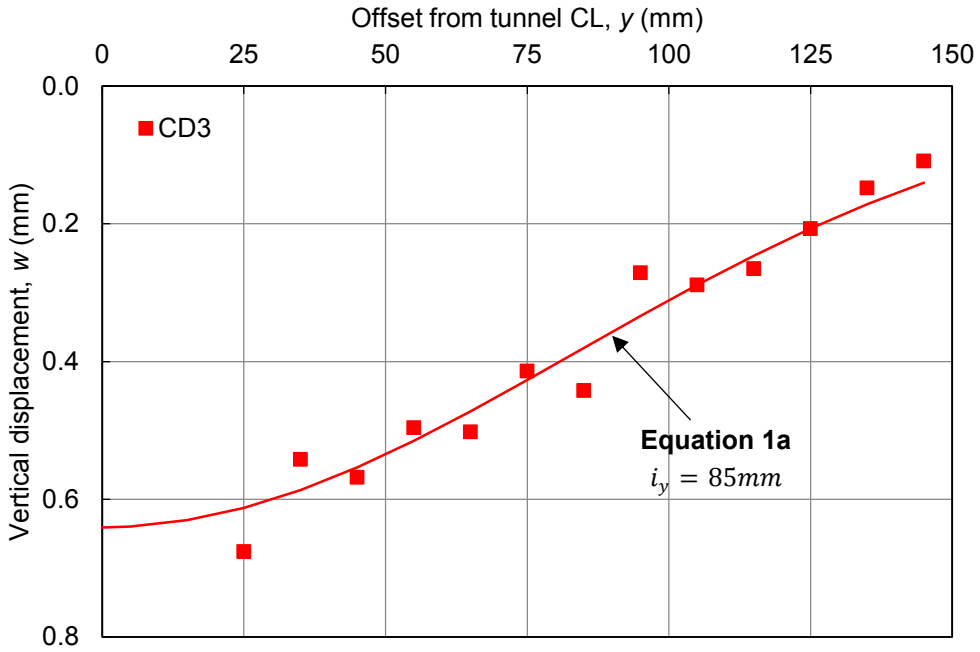

Fig. 4: Typical transverse settlement trough in test CD3.

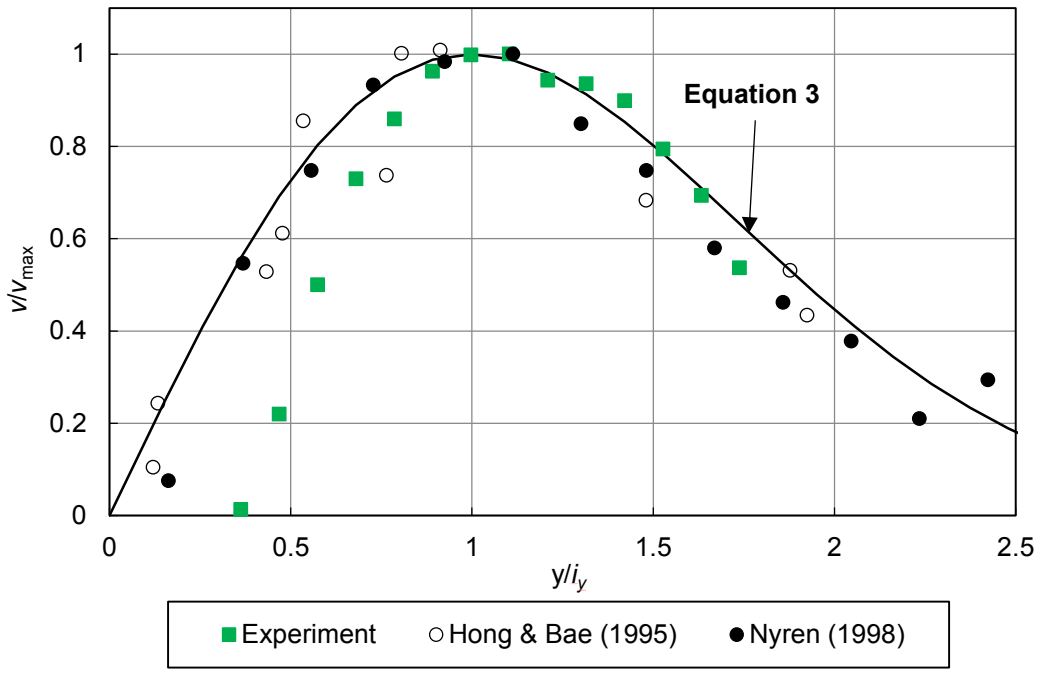

Nyren (1998): data from Total station surface no. 18, west bound

Fig. 5: Transverse surface horizontal soil displacement in test CD3.

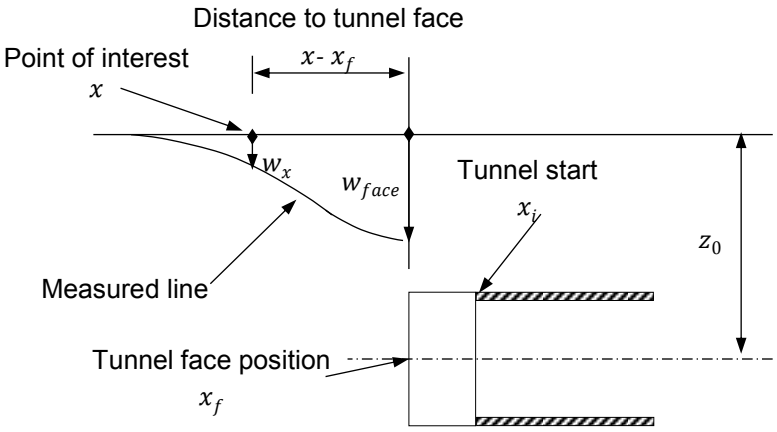

a) Definition of parameters in cumulative function for the centrifuge test setup.

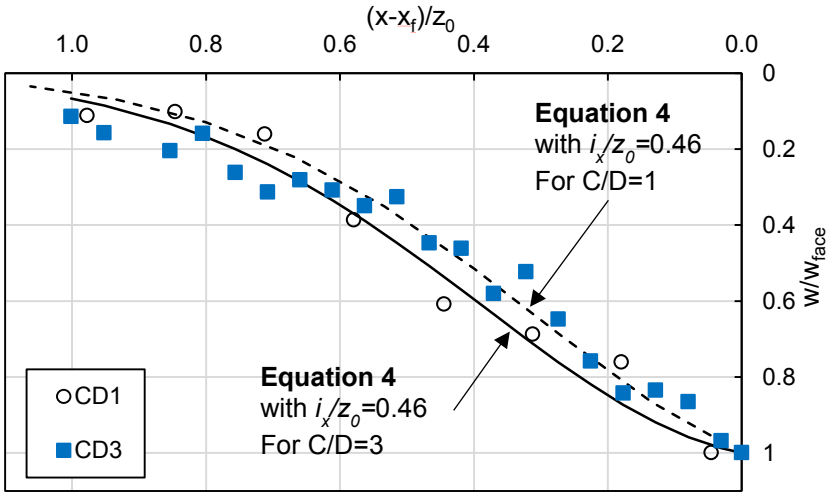

b) Comparison between experimental and empirical data.

Fig 6. Longitudinal surface settlement above tunnel centreline

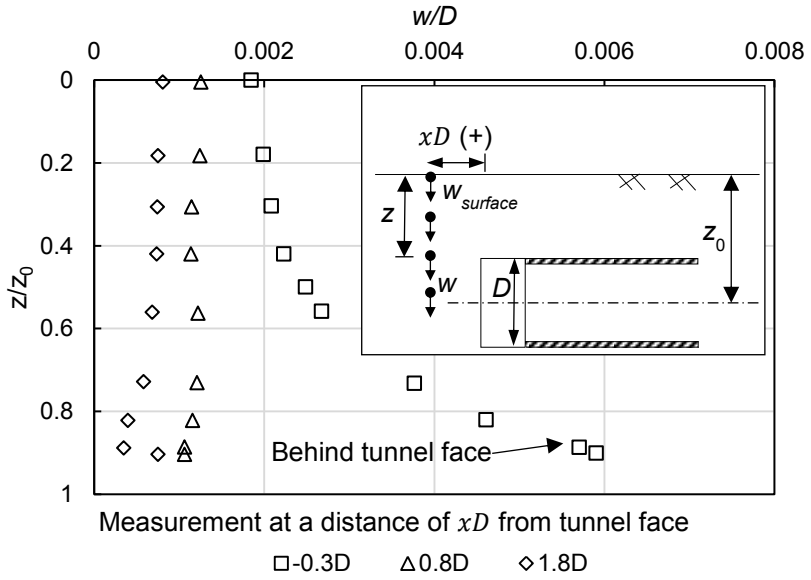

a) West bound tunnel - Nyren (1998)

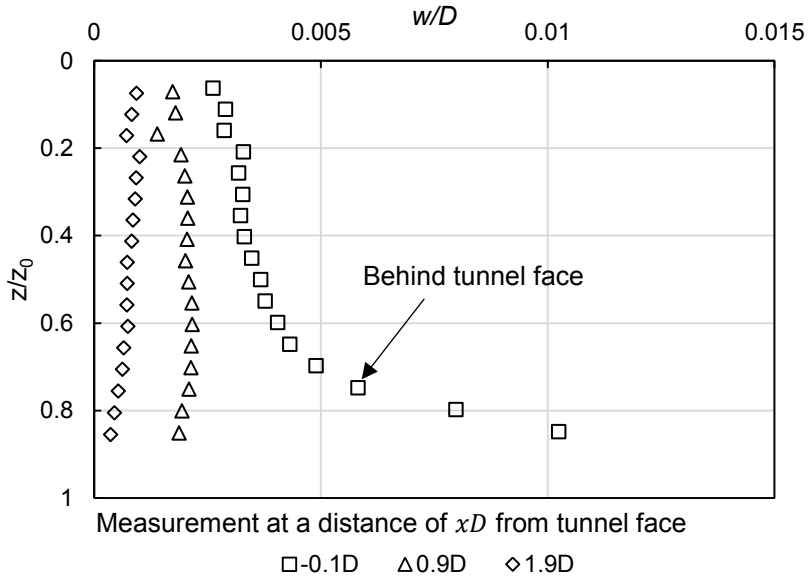

b) Experimental data for test CD3

Fig. 7: Settlement with depth at different locations to tunnel face.

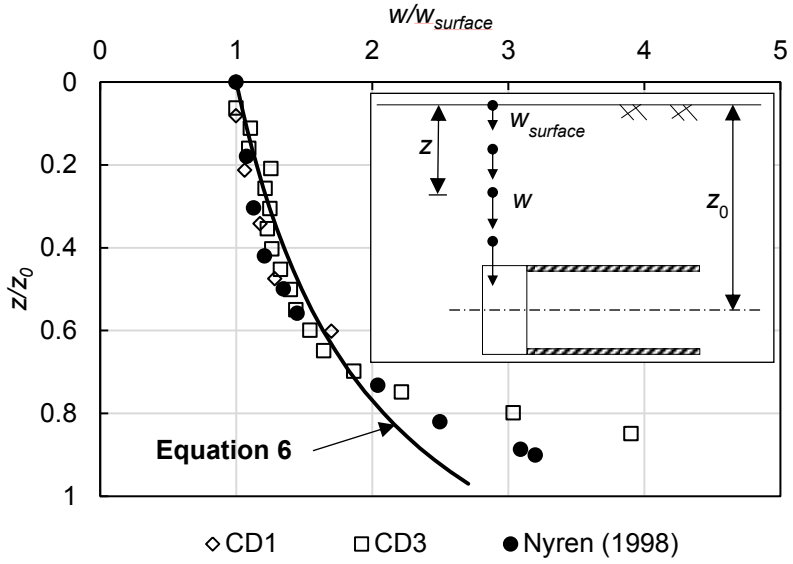

Nyren (1998): data from measurement no 19, west bound

Fig. 8: Settlements with depth behind tunnel face.

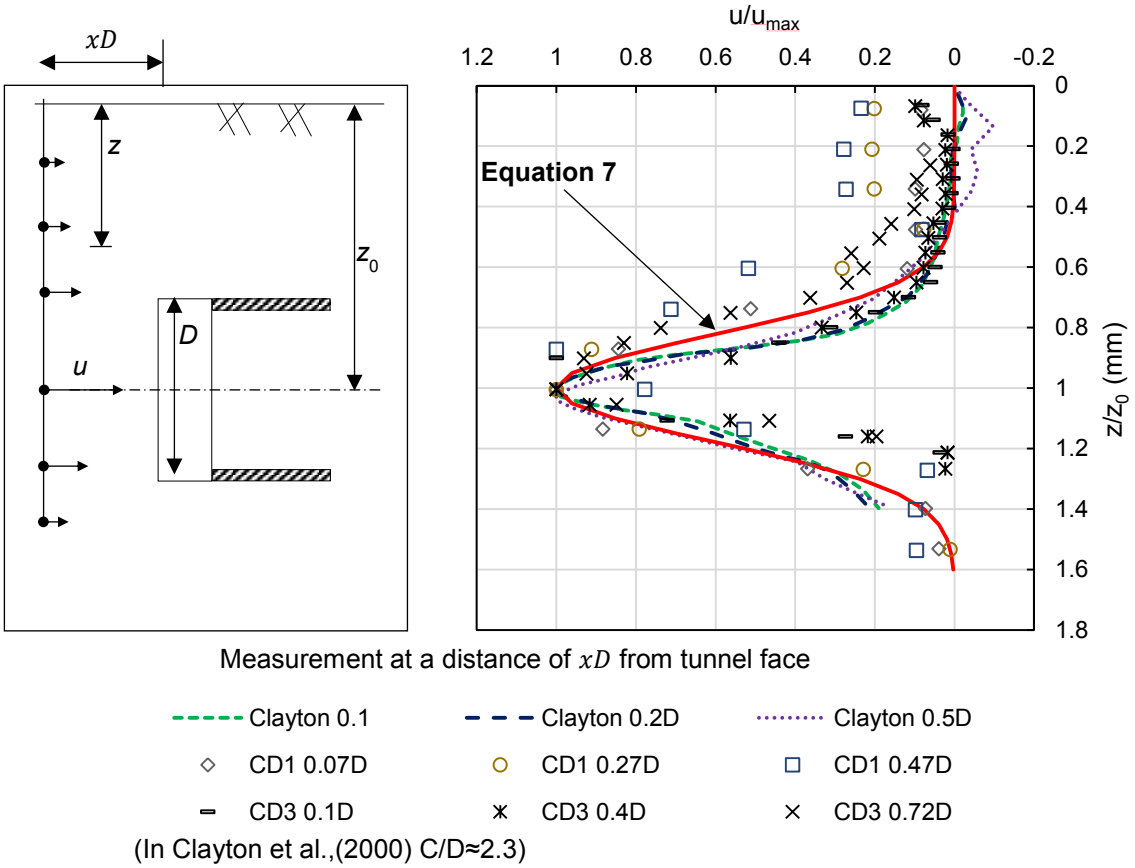

Fig. 9: Horizontal displacement in longitudinal direction.

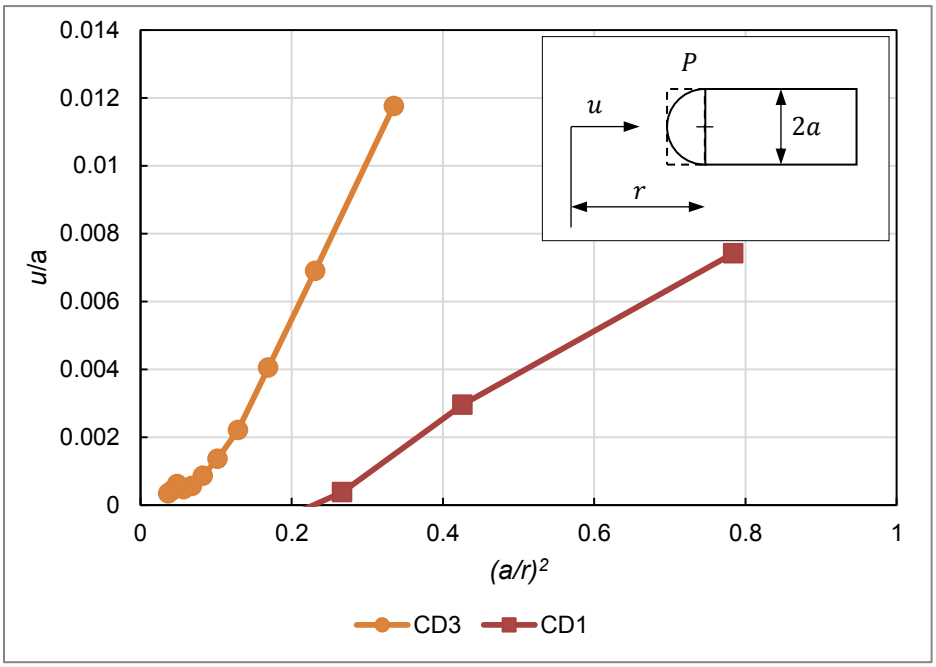

Fig. 10: Horizontal displacement in longitudinal direction at tunnel axis level.

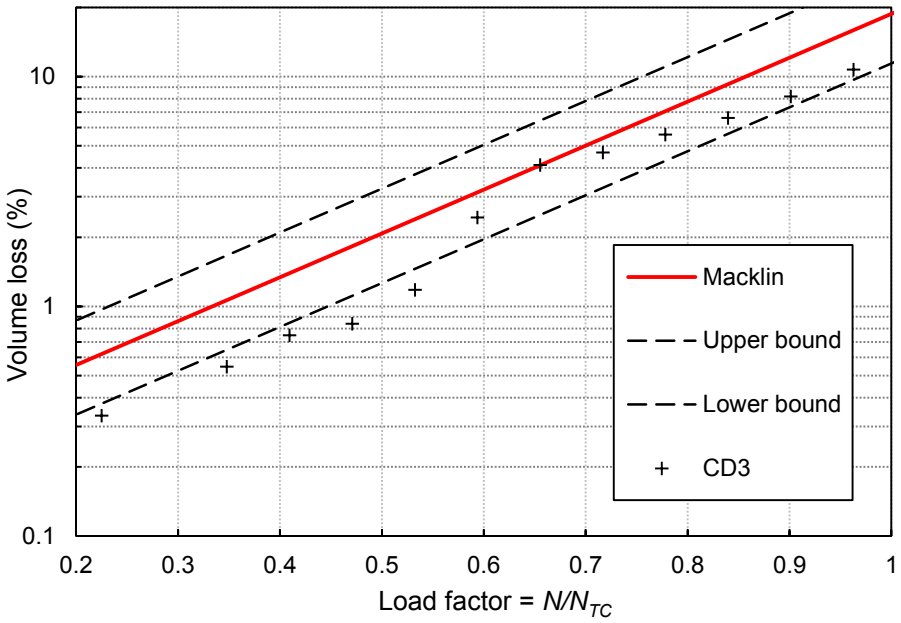

Fig. 11: Relationship of Load Factor, LF and volume loss V_L.